Journal of Earth Science and Engineering 6 (2016) 1-9
doi: 10.17265/2159-581X/2016.01.001

Automated Building Block Extraction and Building Density Classification Using Aerial Imagery and LiDAR Data

Emmanuel Bratsolis[1, 2], Eleni Charou[2, 3], Theocharis Tsenoglou[2] and Nikolaos Vassilas[2]

1. Department of Physics, National University of Athens, Athens 15784, Greece

2. Department of Informatics, Technological Educational Institute of Athens, Aigaleo 12210, Greece

3. Institute of Informatics & Telecommunications, NCSR Demokritos, Agia Paraskevi 15310, Greece

Abstract: This paper examines the utility of high-resolution airborne RGB orthophotos and LiDAR data for mapping residential land uses within the spatial limits of suburb of Athens, Greece. Modern remote sensors deliver ample information from the AOI (area of interest) for the estimation of 2D indicators or with the inclusion of elevation data 3D indicators for the classification of urban land. In this research, two of these indicators, BCR (building coverage ratio) and FAR (floor area ratio) are automatically evaluated. In the pre-processing step, the low resolution elevation data are fused with the high resolution optical data through a mean-shift based discontinuity preserving smoothing algorithm. The outcome is an nDSM (normalized digital surface model) comprised of upsampled elevation data with considerable improvement regarding region filling and "straightness" of elevation discontinuities. Following this step, a MFNN (multilayer feedforward neural network) is used to classify all pixels of the AOI into building or non-building categories. The information derived from the BCR and FAR building indicators, adapted to landscape characteristics of the test area is used to propose two new indices and an automatic post-classification based on the density of buildings.

Key words: Urban density, LiDAR, neural network, classification, land management, building density post-classification.

1. Introduction

Urban density is an important indicator for quality assessment in aspects of urban design, planning and land management. The dispersion of atmospheric pollutants [1], the access of sunlight and solar radiation [2-5], the interior temperatures of buildings [6], the surface thermal conditions [7] are some of the fields affected by the building density. The relationship between the building density of a residential neighborhood and the average wind speed at pedestrian level has been investigated by Kubota et al. [8]. They found that by increasing the building's coverage ratio, the wind speed decreases.

Manually obtaining the heights and shapes of all buildings by on site surveying the area of interest is the traditional method for calculating the BCR (building coverage ratio) and FAR (floor area ratio) indicators. However, in recent years, the LiDAR (light detection and ranging) technology, has efficiently replaced traditional topographic methods for extracting information of urban buildings. Compared to the traditional photogrammetric techniques, the airborne LiDAR provides denser surface elevation samples, over urban areas, even for locations that are inaccessible [9-12]. This, in turn, allows for a more accurate delineation of the footprints of buildings [13-15], and reconstruction of the 3D building shapes [10, 16, 17].

Nevertheless, when the height difference between two surfaces is less than the length of a single laser pulse, LiDAR's capability to distinguish between the two elevations diminishes. Taking full advantage of the capabilities of the LiDAR technology may overcome this problem but requires expensive equipment and

Corresponding author: Emmanuel Bratsolis, Ph.D., research fields: remote sensing and space technology.

complex data processing. An alternative, more economical methodology, is to combine the LiDAR data with data obtained from other sources such as aerial images. In our case, this alternative approach was chosen because we did not have in our disposal precise knowledge about the acquisition of the LiDAR data. We only had a raster file with raw elevation values. For this reason we applied the mean-shift based preprocessing step described in a following section.

For the determination of BCR and FAR indicators based on this approach, the LiDAR data have been effectively combined and used with other data. Yu et al. [18] proposed an automated computation of urban building densities combining LiDAR data and aerial color infrared imagery and an object-based method. Other approaches have also been proposed [19, 20].

In our previous work we proposed an automated method for computing the BCR and FAR urban density indices based on fusing LiDAR data with aerial imagery for one building block [21].

Here we automate our previous work to nine blocks of the same urban region and introduce two new heuristic indices which provide a tool for appraising the quality of housing in different types of residential areas.

The BBDI (building block density index) for post classification of buildings into high, medium and low densities and the BBQI (building block quality index) used to assess the housing quality from low to high quality.

This paper is organized into five sections. Section 2 describes the test area and the data used. Section 3 presents the methodology for the data preprocessing. In Section 4 we introduce the proposed new indices that are based on the BCR and FAR indicators. Finally, Section 5 draws the conclusions.

2. Dataset

For our experiments we consider an area in Kallithea, a suburb of Athens, Greece. The data set consists of aerial orthophotos in the RGB color space (Fig. 1) and LiDAR data of the same area. The orthophotos were obtained from colored aerial imagery (channels Red, Green, Blue) acquired by the National Cadaster and Mapping Agency of Greece. Their spatial resolution is 20 cm and the year of acquisition was 2007. The LiDAR data are in the form of a DSM (digital surface model), containing relative height information of man-made and natural objects rising above the ground at a spatial resolution of 1 m and mean vertical (elevation) resolution of 20 cm. They were, provided by the GeoIntelligence SA, as interpolated elevation values of a point cloud on a uniform rectangular grid. Because the initial data were acquired in 2003, we did not have in our disposal any precise information such as point cloud density or return angle. The lack of this information defined the constraints of our problem. A DTM (digital terrain model) at a spatial resolution of 2 m is also available. Thus, the spatial resolution of the orthophotos is five and ten times higher than that of the DSM and DTM respectively. Both the variations in resolution between color images and elevation data as well as the different acquisition dates pose extra challenges on the processing of our dataset towards the BCR and FAR estimation.

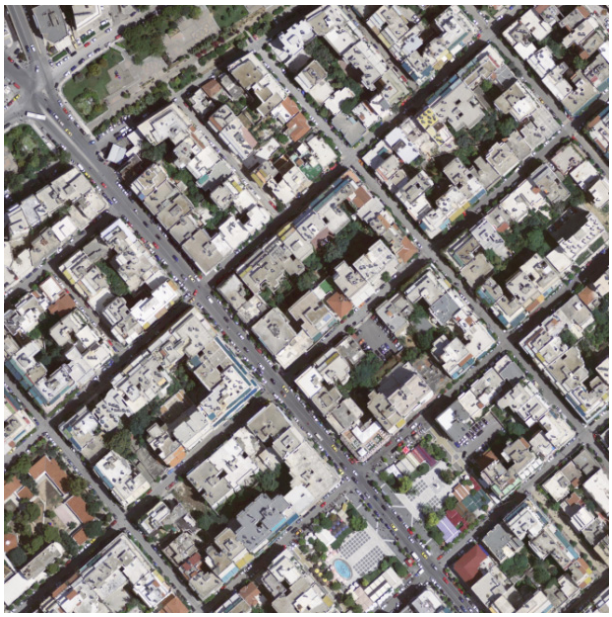

Fig. 1 Original color image.

3. Methodology

3.1 BCR and FAR Indices

The BCR and FAR are the most commonly used indices for quantifying the building density. The BCR is defined as the ratio of the building coverage area (i.e. the area of the building footprint) to the size of land lot:

$$BCR = \frac{S}{S_L} \quad (1)$$

where S is the building coverage area, delineated by the building footprint, and S_L is the area of land lot where the building is located. The BCR measures the building density in 2D (two-dimensional) space.

The FAR is defined as the ratio of gross building floor area to the size of land lot (Eq. (2))

$$FAR = \frac{1}{S_L}\sum_i \frac{H_i}{C} S_i \quad (2)$$

where H_i is the height of the ith building, C is the average height of each floor. As the value of FAR is determined not only by the shape of the building footprint, but also by the vertical distribution of the floors among different heights, it depicts the 3D (three-dimensional) building density. Higher FAR values tend to indicate more urban (dense) construction [18-20].

3.2 Normalization of DSM

Initially, the spatial resolutions of the DTM and DSM are increased to resolution of the color images by performing a nearest neighbor interpolation on each. Then, the nDSM (normalized DSM) is computed as the difference between DSM and the corresponding DTM [22]. Thus the net building heights rather than the absolute elevations are obtained (Fig. 2).

Fig. 2 Normalized DSM (nDSM).

3.3 Mean Shift Application

Because the spatial resolution of our initial elevation data is low, applying a conventional interpolation method to increase their resolution would not give satisfactory results. In our case, the upsampled nDSM obtained in the previous step exhibits strong staircase artifacts near elevation discontinuities caused by the nearest neighbor interpolation. To improve their quality, we use the high detail content of the color image as a guide, fusing the elevation information with the high resolution orthophoto color image.

Given that all images have common georeference, our approach is based on the implicit assumption that the edges of the optical and elevation data are highly correlated. Thus, the color image can provide the necessary information about the significant edges of the scene.

Nevertheless, the optical data also contain a great amount of unnecessary noisy edges caused by uneven painting of the terraces or objects such as solar panels. So, our problem is two-fold: (a) to improve the sharpness of significant elevation edges and (b) to reduce height variations, caused by noise, in areas with flat color content while ignoring small color variations in areas of small elevation differences. To accomplish these goals, we employ a preprocessing technique presented in a previous work [23]. The proposed methodology is autonomous and adaptive.

To improve the quality of the nDSM and eliminate the staircase effects of nearest neighbor upsampling

near elevation discontinuities, we perform a restricted mean shift-based smoothing that selectively preserves the discontinuities on the elevation data. We achieve this, by modifying the mean shift algorithm as proposed by Comaniciu and Meer [24].

The Mean Shift algorithm is a non-parametric, iterative algorithm for finding the local maxima of a density function. It was first proposed by Fukunaga and Hostetler [25]. More recently Comaniciu and Meer introduced it to low-level vision problems. Using a kernel based approximation of the data density the algorithm employs the fixed point iteration to solve the nonlinear optimization problem of locating the maxima (the modes). The iterations may be initialized with random data points of the feature space. Each iteration consists of two steps. In the first step, it computes in the feature space, the point of the highest density in a neighborhood of the current estimate by evaluating the weighted average of the feature values in this neighborhood. The second step is the update step during which the mode estimate is moved towards the point, in the feature space, of highest concentration. These steps are repeated until there is no further modification in the values of the mode estimates. The speed of convergence and the accuracy of the final value depend on the kernel chosen and the size of the neighborhood.

In our case, in contrast to the algorithms presented in Refs. [24, 25], the search for the update values is confined within a spatial neighborhood of the current pixel. At each pixel, our algorithm operates, jointly on the optical and elevation data seeking the most prominent color and elevation values in its spatial neighborhood. The contribution of a neighbor to the computation of the update values depends on its spatial proximity and its color and elevation similarity to the current pixel. Spatially distant neighbors with color or elevation values that differ considerably from the corresponding values of a pixel will contribute less to the computation of the updates of this pixel. Once the iterative process has converged, the final values are assigned to the pixel.

The interdependency-correlation of the color and the elevation values affects the enhancement of the elevation data during the iterative process. Through the joint processing, at each pixel, its color similarity to that of its neighbors controls the kernel-based smoothing of the elevation values in its neighborhood and vice versa. The amount of contribution of a neighbor to the updates is controlled by the form of the kernels used for the averaging and their spread (called the bandwidths). We have chosen all kernels to be of Gaussian form. The bandwidths of the kernels control the distance or degree of variability that a neighboring value is allowed to have in order to contribute to the sum. In our algorithm, color and elevation bandwidths are adapted to the local statistical characteristics of the neighborhood of each pixel. They are computed once, at the beginning of the process, based on the original data. At each pixel their values are the root mean square deviation of the corresponding feature values of the pixel and those of its neighbors.

The algorithm requires from the user to provide only the bandwidth for the spatial kernel, a value which corresponds to actual distance value. This value defines the size of the spatial neighborhood of each pixel. It should be noted that, the update computations can be done in parallel i.e. simultaneously for all pixels. This is because, for each pixel, the computation of the update value depends only on the initial color and elevation values as well as the value computed in the previous iteration for that pixel (i.e., it does not depend on the updated values of the neighboring pixels). It is also worth mentioning that, by the construction of the mean-shift, the size of the update step is adaptive. This helps to avoid oscillatory phenomena or slow convergence, contributing to the efficiency of the algorithm.

Nevertheless, as the iterations progress, data interdependency-coupling will inevitably cause over-smoothing of important edges. To control it we

have introduced an additional constraining factor. It also has a Gaussian form and its argument depends on the color difference between a pixel and those of its neighbors in the initial image. It allows neighboring pixels with small (spurious) color variations in the original data to merge while it prevents merging when the initial color variations are larger than certain threshold. That way it counterbalances the gradual smoothing of the data values caused by the iterative process. The threshold defines the bandwidth (spread) of the kernel and depends on the direction, thus making this factor anisotropic. For each direction, formed by the center pixel and one of its neighbors, the bandwidth is the root mean square over the whole image of the color difference between pixels in the same direction.

The results are shown in Figs. 3 and 4 for nine of the building blocks that were used for the evaluation of the BCR and FAR indices. These figures show that despite the clutter present in the color image and the poor quality of the elevation data, our algorithm was robust because it was able to automatically adapt its parameters to the local characteristics of the data.

Specifically, the outcome is on the one hand a more homogeneous RGB image, with smoothed terrace coloring while at the same time preserving the optical edges and on the other hand an elevation image with much straighter height discontinuities that has gained significantly in detail and sharpness with the different elevation surfaces becoming much better discriminated (Fig. 4). It is worth noting that edges in the color image (such as shadows edges) that do not correspond to significant elevation variations do not appear in the resulting elevation image.

Fig. 3 Result of mean-shift edge-preserving smooth-ing on color image.

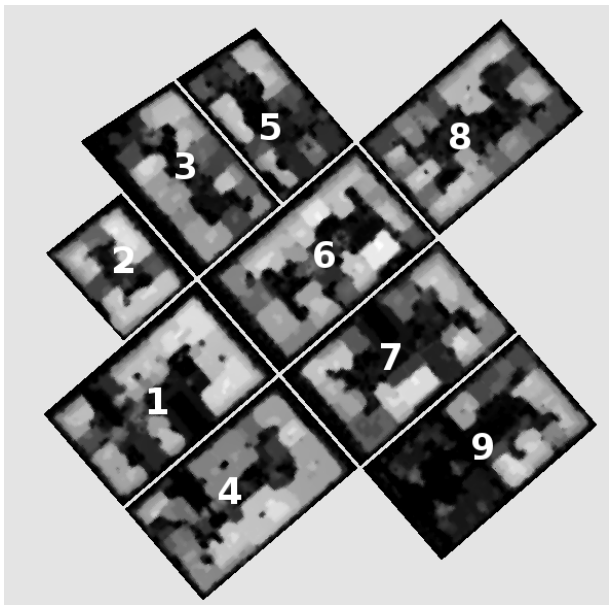

Fig. 4 nDSM after the application of mean-shift jointly on color and elevation data.

3.4 Thresholding

An appropriate base building height (H_0) is selected as the threshold value to segment the mean-shifted nDSM and to extract the buildings. If the base building height H_0 is too high, true buildings will be missed. On the other hand, if the selected base building height H_0 is too low, some small nonbuilding objects like automobiles will be detected as buildings. Different threshold values have been chosen to extract building objects in previous studies, e.g., 3 m by Ma [11], 3.5 m by Yu et al. [18] and 4 m by Yu et al. [14, 22]. After experimenting with different threshold values we chose 3 m as the threshold for our case study.

3.5 Neural Network Based Classification

According to our previous investigation [23, 26] automatic segmentation into buildings-nonbuildings could be efficiently performed using a MFNN (multilayer feedforward neural network) having as input the result of the Mean-Shift-based preprocessing step. The input layer consists of four nodes: 3 nodes for the 3 color channels (red, green, blue) and 1 node for the thresholded elevation values (i.e. the result of subsection 3.3).

The network was trained with the Levenberg-Marquardt algorithm [27]. Following experimentation with several architectures we eventually selected a network with two hidden layers of 50 and 10 neurons respectively. The training data were selected by the user using scribbles.

The training process was designed to avoid overtraining. Overtraining is a well-known problem in neural network training and is due to a high tuning of the artificial neural networks on the examples of the training set, usually resulting in poor generalization. To alleviate this problem, the data set is split into a training set and a validation set. While the training set is used to train the networks, the validation set is used to evaluate the network's performance at regular steps during the training phase. Training is stopped when the performance on the validation set is maximized. The training, validation and testing sets included a total of 58,744 pixels (less than 2% of all pixels) of which 41,121 for training, 8,111 for validation and 8,112 for testing, along with their correct classification. They have been extracted from a different region of Kallithea suburb by specifying small polygons representing the two classes: buildings and non-buildings. The output of the classifier is a grayscale image with values varying from 1 (building) to 0 (non building). We convert this image into a binary image using a threshold value of 0.2 thus rejecting any noisy classification values (Fig. 5).

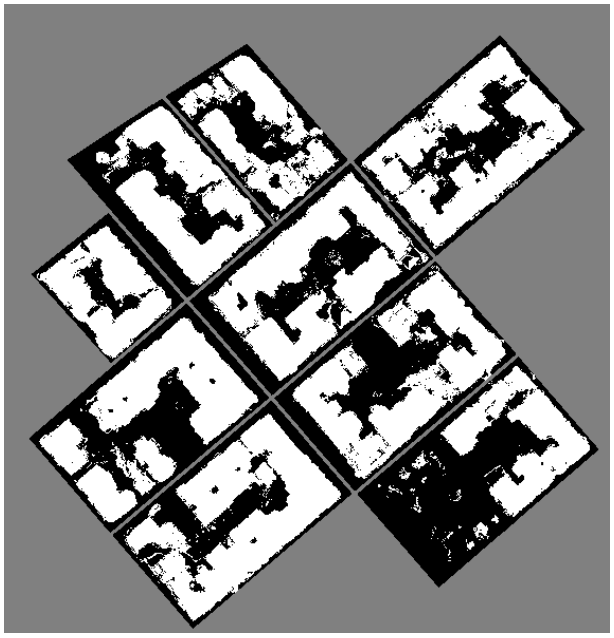

Fig. 5 Two-class NN classification results: building (white regions); nonbuilding (black regions).

4. Building Block Density and Quality Indices

Our approach for evaluating the BCR and FAR indices was performed on nine city blocks that are fully contained in the data.

These blocks are shown in the color image (Fig. 3) and in the nDSM (Fig. 4), where they are also numbered, after these images have undergone edge preserving smoothing. The separation of the blocks was done manually. Fig. 5 shows the classification mask used to distinguish between the areas covered by buildings (white) and non-buildings (black). Referring to Fig. 5, BCR for each block is computed as the ratio of the white area divided by the total area of the block (sum of white and black areas). To compute FAR, for each white pixel of Fig. 5 we refer to the corresponding elevation in Fig. 4. The values of the indices for each block are shown in Table 1. The first column refers to the block numbering of Fig. 4.

To define the BBDI and the BBQI, based on the BCR and FAR indicators, along the line of a previous work [28], we apply the following empirical rule:

Table 1 BCR and FAR values for the nine building blocks of Figs. 3-5 and the corresponding values of the proposed BBDI and BBQI.

Building block No.	BCR	FAR	BBDI	BBQI
1	0.55	3.11	Medium	Medium
2	0.65	3.48	High	Low
3	0.56	2.56	Medium	Medium
4	0.63	3.21	High	Low
5	0.54	2.05	Medium	Medium
6	0.59	3.23	Medium	Medium
7	0.55	2.60	Medium	Medium
8	0.61	2.76	Medium	Medium
9	0.33	1.50	Low	High

- If BCR <= 0.5 and FAR <= 1.5, then BBDI is low and BBQI is high;
- If BCR > 0.6 and FAR > 3, then BBDI is high and BBQI is low;
- For all other cases, BBDI and BBQI are medium.

These results are summarized in Table 1.

5. Conclusions

Two are the main contributions of this work. First, we present an adaptive method for the detection and extraction of building blocks embedded in a dense urban environment. Subsequently, based on the previous step, we propose two indices for the classification of buildings that can be used to assess the quality of habitation.

The proposed iterative, data adaptive, method is based on the mean shift algorithm. Through the joint feature update, the algorithm is able to fuse optical and elevation data resulting in a qualitative improvement of both: the optical RGB data through edge-preserving smoothing and the elevation (nDSM) data through edge-preserving upsampling. To this end, we introduce an extra edge enhancing factor to counterbalance the smoothing effect of the iterative process. The resulting elevation data displayed considerable improvement regarding region filling and the sharpness of discontinuities.

Nine building blocks used in our evaluation experiments were extracted from processed elevation data using an artificial neural network which classified all pixels of the AOI into building or non-building categories. The proposed BBDI and BBQI combined information derived from the BCR and FAR urban density indicators based on a set of heuristic rules compatible with the landscape of the specific Athenian suburb of Kallithea.

The processing steps presented could be applied in cases where limited information is available about elevation data of low spatial resolution. Future work could be devoted to investigate improvements in feature selection and extraction to overcome is lack of information.

Acknowledgment

This research has been co-funded by the European Union (European Social Fund) and Greek national resources under the framework of the Archimedes III: Funding of Research Groups in T.E.I. of Athens Project of the Education & Lifelong Learning Operational Program. We would also like to thank GeoIntelligence for providing the DSM and DTM elevation data as well as the National Cadastre & Mapping Agency of Greece for providing us with the high resolution aerial photographs.

References

[1] Theodoridis, G., and Moussiopoulos, N. 2000. “Influence of Building Density and Roof Shape on the Wind and dispersion characteristics in an Urban Area: A Numerical Study.” *Environmental Monitoring and Assessment* 65 (1-2): 407-15.

[2] Lam, J. C. 2000. "Shading Effects Due to Nearby Buildings and Energy Implications." *Energy Conversion and Management* 41 (7): 647-59.

[3] Miguet, F., and Groleau, D. 2002. "A Daylight Simulation Tool for Urban and Architectural Spaces—Application to Transmitted Direct and Diffuse Light through Glazing." *Building and Environment* 37 (8-9): 833-43.

[4] Oke, T. R. 1988. "Street Design and Urban Canopy Layer Climate." *Energy and Buildings* 11 (2): 103-13.

[5] Yu, B., Liu, H., Wu, J., and Lin, W. M. 2009a. "Investigating Impacts of Urban Morphology on Spatio-Temporal Variations of Solar Radiation with Airborne LiDAR Data and a Solar Flux Model: A Case Study of Downtown Houston." *International Journal of Remote Sensing* 30 (17): 4359-85.

[6] Mills, G. 1997. "Building Density and Interior Building Temperatures: A Physical Modeling Experiment." *Physical Geography* 18 (3): 195-214.

[7] Streutker, D. R. 2003. "Satellite-Measured Growth of the Urban Heat Island of Houston, Texas." *Remote Sensing of Environment* 85 (3): 282-9.

[8] Kubota, T., Miura, M., Tominaga, Y., and Mochida, A. 2008. "Wind Tunnel Tests on the Relationship between Building Density and Pedestrian-Level Wind Velocity: Development of Guidelines for Realizing Acceptable Wind Environment in Residential Neighborhoods." *Building and. Environment* 43 (10): 1699-708.

[9] Gamba, P., and Houshmand, B. 2000. "Digital Surface Models and Building Extraction: A Comparison of IFSAR and LIDAR Data." *IEEE Transactions on Geosciences and Remote Sensing* 38 (4): 1959-68.

[10] Gamba, P., and Houshmand, B. 2002. "Joint Analysis of SAR, LIDAR and Aerial Imagery for Simultaneous Extraction of Land Cover, DTM and 3D Shape of Buildings." *International Journal of Remote Sensing* 23 (20): 4439-50.

[11] Priestnall, G., Jaafar, J., and Duncan, A. 2000. "Extracting Urban Features from LiDAR Digital Surface Models." *Computers, Environment and Urban Systems* 24 (2): 65-78.

[12] Stilla, U., Soergel, U., and Thoennessen, U. 2003. "Potential and Limits of InSAR Data for Building Reconstruction in Built-up Areas." *ISPRS Journal of Photogrammetry and Remote Sensing* 58 (1-2): 113-23.

[13] Ma, R. J. 2005. "DEM Generation and Building Detection from Lidar Data." *Photogrammetric Engineering and Remote Sensing* 71 (7): 847-54.

[14] Yu, B., Liu, H., Zhang, L., and Wu, J. 2009b. "An Object-Based Two-Stage Method for a Detailed Classification of Urban Landscape Components by Integrating Airborne LiDAR and Color Infrared Image Data: A Case Study of Downtown Houston." *Joint Urban Remote Sensing Event (JURSE),* Shanghai.

[15] Zhang, K., Yan, J., and Chen, S. C. 2006. "Automatic Construction of Building Footprints from Airborne LiDAR data." *IEEE Transactions on Geosciences and Remote Sensing* 44 (9): 2523-33.

[16] Forlani, G., Nardinocchi, C., Scaioni, M., and Zingaretti, P. 2006. "Complete Classification of Raw LiDAR Data and 3D Reconstruction of Buildings." *Pattern Analysis and Applications* 8 (4): 357-74.

[17] Rottensteiner, F. 2003. "Automatic Generation of High-Quality Building Models from LiDAR Data." *IEEE Computer Graphics and Applications* 23 (6): 42-50.

[18] Yu, B., Liu, H., Wu, J., Hu, Y., and Zhang, L. 2010. "Automated Derivation of Urban Building Density Information Using Airborne LiDAR Data and Object-Based Method." *Landscape and Urban Planning* 98: 210-9.

[19] Pan, X. Z., Zhao, Q. G., Chen, J., Liang, Y., and Sun, B. 2008. "Analyzing the Variation of Building Density Using High Spatial Resolution Satellite Images: The Example of Shanghai City." *Sensors* 8: 2541-50.

[20] Suparwoko, I. M. 2013. "Green Open Space Approach to the Building Mass Arrangement in Yogyakarta: Case Study of the Revitalization of the Tugu Rail Station." *International Journal of Civil & Environmental Engineering* 13 (4): 1-8.

[21] Charou E., Gyftakis, S., Bratsolis, E., Tsenoglou, T., Papadopoulou, Th. D., and Vassilas, N. 2015. "Urban Density Indices Using Mean-Shift-Based Upsampled Elevation Data." *36th International Symposium on Remote Sensing of Environment, (ISRSE)* 36-428-1, 11-15 May, Berlin, Germany.

[22] Haala, N., and Brenner, C. 1999. "Extraction of Buildings and Trees in Urban Environments." *ISPRS Journal of Photogrammetry and Remote Sensing* 54 (2-3): 130-7.

[23] Gyftakis, S., Tsenoglou. T., Bratsolis, E., Charou, E., and Vassilas, N. 2014. "Fusion of Aerial Images with Mean Shift-Based Upsampled Elevation Data for Improved Building Block Classification." *SPIE Remote Sensing* 9244: 1-10.

[24] Comaniciu, D., and Meer, P. 2002. "Mean Shift: A Robust Approach toward Feature Space Analysis." *IEEE Transactions on Pattern Analysis and Machine Intelligence* 24 (5): 603-19.

[25] Fukunaga, K., and Hostetler, L. D. 1975. "The Estimation of the Gradient of a Density Function, with Applications in Pattern Recognition." *IEEE Transactions on Information Theory* 21: 32-40.

[26] Bratsolis, E., Gyftakis, S., Charou, E., and Vassilas, N. 2013. "Comparative Analysis of Classification Techniques for Building Block Extraction Using Aerial

Imagery and LiDAR Data." *Proceedings of 13th IEEE International Symposium on Signal Processing and Information Technology (ISSPIT)*: 80-5.

[27] Haykin, S. 1994. "Neural Networks: A Comprehensive Foundation." Macmillan, New York.

[28] Alhaddad, B. I., Roca, J., Burns, M. C., and Garcia, J. 2008. "Satellite Imagery and LiDAR Data for Efficiently Describing Structures and densities in Residential Urban Land Uses Classification." *Proceedings of ISPRS*, Beijing.

Algorithmic Steps of Preprocessing

(1) Compute values of smoothing factor (Eq. (3));

(2) Read data from neighborhood of current pixel;

(3) Compute kernels: D for distance, C for color and E for elevation;

(4) Compute normalization factor K_j (Eq. (4));

(5) Update according to Eq. (5);

(6) Repeat steps 2-5 until convergence.

$$\xi_{j,i} = F\left(\frac{\left\|z_j^c - z_i^c\right\|}{h_g(j,i)}\right) \tag{3}$$

$$K_j = \sum_i C\left(\frac{\left\|x_j^c(n) - z_i^c\right\|}{h_c(i)}\right) E\left(\frac{\left\|x_j^e(n) - z_i^e\right\|}{h_e(i)}\right) D\left(\frac{\|j-i\|}{h_s(i)}\right) \xi_{j,i} \tag{4}$$

$$\begin{bmatrix} x_j^c(n+1) \\ x_j^e(n+1) \end{bmatrix} = \frac{1}{K_j} \sum_i \begin{bmatrix} z_i^c \\ z_i^e \end{bmatrix} C\left(\frac{\left\|x_j^c(n) - z_i^c\right\|}{h_c(i)}\right) E\left(\frac{\left\|x_j^e(n) - z_i^e\right\|}{h_e(i)}\right) D\left(\frac{\|j-i\|}{h_s(i)}\right) \xi_{j,i} \tag{5}$$

Where: i, j are pixel indices;

n is the iteration index;

z^c, $x^c$are the initial and current color;

z^e, $x^e$are the initial and current elevation.

h: are the corresponding bandwidths